T-cell motility in the early stages of the immune response modeled as a random walk amongst targets

S. P. Preston, S. L. Waters,* and O. E. Jensen
Centre for Mathematical Medicine, School of Mathematical Sciences, University of Nottingham, University Park, Nottingham NG7 2RD, United Kingdom

P. R. Heaton
WALTHAM Centre for Pet Nutrition, Freeby Lane, Waltham-on-the-Wolds, Melton Mowbray, Leics LE14 4RT, United Kingdom

D. I. Pritchard
School of Pharmacy, University of Nottingham, University Park, Nottingham NG7 2RD, United Kingdom
(Received 15 March 2006; published 17 July 2006)

The transport process by which a T cell makes high-frequency encounters with antigen-presenting cells following infection is an important element of adaptive immunity. Recent experimental work has allowed *in vivo* cell motility to be characterized in detail. On the basis of experimental data we develop a quantitative model for encounters between T cells and antigen-presenting cells. We model this as a transport-limited chemical reaction with the dynamics dependent on physical contact between randomly moving reactants. We use asymptotic methods to calculate a time distribution which characterizes the delay before a T cell is activated and use Monte Carlo simulations to verify the analysis. We find that the density of antigen-primed dendritic cells within the lymph node paracortex must be greater than 35 cells/mm^3 for a T cell to have a more than 50% chance of encountering a dendritic cell within 24 h. This density is much larger than existing estimates based on calculations which neglect the transport process. We also use simulations to compare a T cell which re-orients isotropically with a T cell which turns according to an experimentally observed distribution and find that the effects of anisotropy on the solution are small.

DOI: 10.1103/PhysRevE.74.011910 PACS number(s): 87.17.Aa, 82.39.−k, 82.20.Fd

I. INTRODUCTION

Within an individual, the population of lymphocytes is highly diverse, enabling the immune system to respond to almost any potential antigen. A consequence of maintaining this diversity is that only a few lymphocytes are specific to an unfamiliar antigen. Hence a key feature of adaptive immunity is the dramatic clonal expansion of antigen-specific lymphocytes which follows infection.

Once antigen enters the body it is taken up by antigen-presenting cells (APCs) near the site of infection. These APCs then migrate to lymphoid tissue such as lymph nodes, where lymphocytes are found in high concentrations. The APCs remain there for some time displaying antigenic peptides on their surface. Alternatively, soluble antigens drain from peripheral tissue into lymph and are advected along lymphatic vessels until they enter the draining lymph node. Soluble antigen is taken up and presented inside the lymph node by a subset of APCs called dendritic cells (DCs) [1–3].

Lymphocytes are produced from haematopoietic stem cells in the bone marrow. Lymphocytes which mature in the bone marrow are called B cells; these cells are responsible for producing antibody. Lymphocytes which migrate and mature in the thymus are known as T cells. T cells are further subclassified according to expression of the surface glycoproteins CD4 and CD8. There are distinct functional differences between the two classes: CD4 T cells are responsible for regulating the B cell response, whereas CD8 T cells detect and destroy virally infected cells. Thus T cells are fundamental in almost all immune responses.

Before a T cell can proliferate it must make physical contact with an APC which displays the appropriate antigen. When a T cell encounters an APC, a transient structure known as a synapse is formed between the cells, across which information is exchanged. The synapse facilitates antigen surveillance by the T cell and is a necessary stimulus to activate T-cell proliferation. However, the number of antigen-specific precursor T cells in the repertoire is very small; for example, in the repertoire of mice only around 1 in 10^5 to 10^6 CD8 T cells is specific upon infection by an unfamiliar antigen [4,5]. Hence it is a considerable challenge to ensure this tiny subset of cells receives the stimulation necessary to initiate the immune response.

It has long been understood that the lymph node (depicted in Fig. 1) provides an optimal environment for generating and maintaining adaptive immunity, but only in recent years has it become possible to view inside the lymph node and observe the behavior of lymphocytes and DCs as they function *in vivo*. Researchers using multiphoton microscopy have imaged murine immune cells deep below the surface of intact lymph nodes, revealing that lymphocytes and DCs are both highly active in promoting encounters with one another [5–10]. T cells, which are predominantly found in the paracortex (see Fig. 1), are highly motile, crawling with a mean velocity $\approx 11\ \mu\mathrm{m\ min}^{-1}$ and achieving peak velocities

*Author to whom correspondence should be addressed. Electronic address: sarah.waters@maths.nottingham.ac.uk

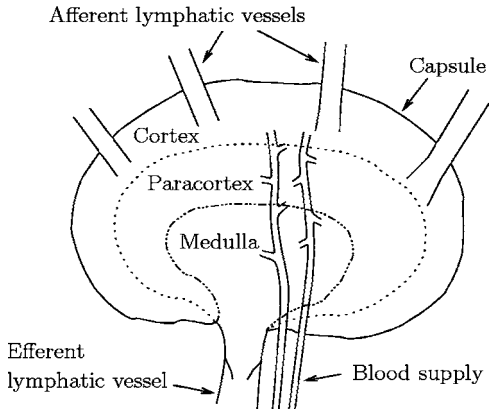

FIG. 1. Diagram showing the histological regions of a typical lymph node. Antigen enters through the afferent lymphatic vessels and is sequestered by DCs. T cells enter via the blood and survey antigen-bearing DCs in the paracortex.

$>25\ \mu\mathrm{m\ min}^{-1}$. Some dendritic cells are also motile (mean velocity $\approx 2-3\ \mu\mathrm{m\ min}^{-1}$) and can move their dendrites at velocities up to $\approx 40\ \mu\mathrm{m\ min}^{-1}$ to increase the cells' "effective volume" and thus their capacity to make contact with surveying T cells [8]. The important physical parameters in this process are summarized in Table I.

Remarkably, there is convincing evidence that both T cells and DCs move randomly without directional bias [5–9], contrary to the notion that cell movement is strategically coordinated by the lymph node architecture [1], or that chemotaxis is involved in directing T cells to antigen-bearing DCs. This experimental evidence has led to the view that immune surveillance by the T-cell repertoire is a stochastic process, resulting from chance encounters between T cells and DCs [11]. Although it is not universally accepted (Castellino *et al.* [10] have recently shown that chemokines may indeed bias T-cell trajectories), throughout this paper we follow the stochastic view and regard T-cell movement to be random and undirected.

Imaging techniques are also leading to an improved understanding of how antigen presentation occurs *in vivo*. Multiphoton microscopy studies [5–10,12] complement tissue sectioning and confocal microscopy [13,14] to provide a more complete picture of the early stages of the immune response. Data from imaging studies have been used by Catron *et al.* [15], who created spatially and temporally scaled simulations of a two-dimensional cross section of a lymph node. These simulations depict the immune response in the first few days after infection to show how cell motility results in T-cell–DC encounters.

TABLE I. Summary of parameters relating to cell motility and the lymph node.

Parameter	Value	Source
Surface area of dendritic cell	$1800-2400\ \mu\mathrm{m}^2$	[8]
Radius of dendritic cell, r_d	$20-25\ \mu\mathrm{m}$	[8]
Mean velocity of dendritic cell, s_d	$2\ \mu\mathrm{m\ min}^{-1}$	[8]
Peak velocity of dendrites	$40\ \mu\mathrm{m\ min}^{-1}$	[8]
Radius of naive T cell, r_t	$3.5\ \mu\mathrm{m}$	[1]
Mean velocity of T cell, s_t	$11\ \mu\mathrm{m\ min}^{-1}$	[7]
Peak velocity of T cell	$>25\ \mu\mathrm{m\ min}^{-1}$	[7,8]
Mean rate of T cell turns, λ	$0.5\ \mathrm{min}^{-1}$	[7]
Lymph node diameter	$1-20$ mm	[17]

Understanding cell activation and proliferation is key to developing larger models of the immune response. Since an early model proposed by Bell [16], many authors have modeled immune dynamics using coupled nonlinear ordinary differential equations (ODEs). ODE models are appealing because they are straightforward to solve and their qualitative behavior is consistent with experimental observations. However, such models also have many limitations.

First, the ODEs are generally a deterministic description of an underlying stochastic process; the dependent variables in the ODEs are averaged quantities which neglect spatial variation. This assumption is hard to reconcile with an adaptive immune system whose function relies strongly on its spatial structure. Second, when the number of reactants is small then stochastic fluctuations are too large to neglect and in these circumstances the deterministic description is poor. Deterministic descriptions are especially weak in the early stages of an immune response when there are very few antigen-specific cells. If we wish to consider a single precursor cell then the "precursor cell concentration" is ill-defined and the deterministic description becomes meaningless. A third criticism is that ODE models often contain a large number of parameters which are difficult to measure experimentally.

We avoid these problems by adopting an alternative approach. In this paper we formulate a mathematical model of the transport process by which a T cell encounters a DC to initiate an immune reaction, by analyzing a single T cell and using parameters which have been reported experimentally.

The problem of an immune reaction which depends on contact between T cells and DCs is analogous to a chemical reaction in solution, where reaction occurs only when the diffusing reactants collide. Such diffusion-limited reactions have been extensively studied due to their wide-ranging applications [18]. The early analysis by Smoluchowski [19] first proposed a method of calculating the rate coefficient of an ODE in terms of the diffusion coefficients of the reactants. More recently Tachiya [20] showed that Smoluchowski's solution could be derived by analyzing the reaction probability of isolated pairs of diffusing reactants.

The aim of this paper is to quantify how long it takes for T cells to become activated; this time is of practical interest to immunologists but is very difficult to measure experimentally. Our approach is to model T cells as random walkers and DCs as stationary targets. In Sec. II we extend Tachiya's diffusion theory to calculate the activation time for a T cell which moves according to a fixed-speed "velocity-jump" equation [21]. Consistent with experimental evidence which shows that T cells move in discrete lunges [6,9], the random-walk model assumes that the walker moves in straight line segments, and between segments re-orients itself randomly. We show in Sec. III that the Smoluchowski diffusion solu-

tion is a leading-order solution of our model which holds for large time, under appropriate conditions. We also calculate higher-order corrections to give improved accuracy at intermediate times, and compare our solution with results from Monte Carlo simulations. Our analysis makes explicit both the assumptions on which the solution is based and the dependence of the solution on experimentally measurable parameters. In Sec. III D we estimate the number of DCs required for a successful immune response and we compare this figure with an existing estimate from the literature. In Sec. III E we use simulations to compare the solution for a walker which re-orients isotropically between steps with the solution for a walker which re-orients according to an experimentally observed turning distribution. We discuss in Sec. IV the validity of our modeling assumptions and how they may be relaxed in the future.

II. MATHEMATICAL MODEL

Following an infection we suppose that a small subset of T cells within the local lymph node are antigen-specific. We consider a single antigen-specific T cell and henceforth refer to this as the "walker." The lymph node contains many DCs of which some fraction express peptides of the infecting antigen. DCs which do not bear antigen are subsequently neglected, whereas antigen-bearing DCs are termed "targets." We assume that the targets lie within the lymph node paracortex, and we denote this domain by Γ.

Our aim is to calculate the time taken for a walker to encounter a target. Borrowing a phrase from the chemical reaction literature, we call this time the "survival time" and denote it by τ. Because the movement of walkers and the distribution of targets are random, τ is itself a random variable which is characterized by the distribution

$$\mathrm{Prob}\{\tau > t\}, \tag{1}$$

which we term the "survival probability." Our objective is to calculate this probability distribution.

We may assume without loss of generality that the walker is centered initially at the origin and we suppose there are N targets centered at $\mathbf{x}_{0_1}, \mathbf{x}_{0_2}, \ldots, \mathbf{x}_{0_N}$. The survival probability for the walker amongst this configuration of targets is written $S_N(t;\mathbf{x}_{0_1}, \mathbf{x}_{0_2}, \ldots, \mathbf{x}_{0_N})$. Provided the concentration of targets is sufficiently small and the targets are not clustered then the survival probability can be factored as

$$S_N(t;\mathbf{x}_{0_1}, \mathbf{x}_{0_2}, \ldots, \mathbf{x}_{0_N}) = \prod_{i=1}^{N} S(t;\mathbf{x}_{0_i}). \tag{2}$$

This factorization (discussed by Weiss [22] and in references therein) neglects competition between targets to make first contact with the walker; the competition is a so-called "many-body" effect and Berezhkovskii *et al.* [23] have shown, in the case where the targets are stationary, that the solution obtained using Eq. (2) is a lower bound on the exact solution. The many-body effects become less pronounced as the dimensionality of space increases and as the concentration of targets decreases. For problems in three spatial dimensions with targets distributed sufficiently sparsely then the factorization provides a good approximation [23,24].

Equation (2) simplifies the problem considerably; the task of calculating the survival probability of a walker amongst numerous targets reduces to the much easier task of calculating the survival probability of a walker from a single target.

Supposing that the targets are uniformly distributed in Γ then the spatially averaged survival probability $\hat{S}(t)$ from a single target is

$$\hat{S}(t) = \int_{\Gamma} S(t;\mathbf{x}_0) d^3\mathbf{x}_0 / |\Gamma|, \tag{3}$$

where $|\Gamma|$ is the volume of Γ. Thus from Eq. (2) we have

$$\hat{S}_N(t) = [\hat{S}(t)]^N. \tag{4}$$

Equation (4) provides an effective means of calculating the spatially averaged survival probability when the number of targets, N, is small. When N is large and the domain Γ over which the targets reside is also large then it is more convenient to use the asymptotic approximation $N, |\Gamma| \to \infty$ [20]. In this case we may work in terms of the concentration c of targets,

$$c = \lim_{N,|\Gamma|\to\infty} N/|\Gamma|, \tag{5}$$

where c is a finite constant. Then the survival of a walker in an asymptotically large domain containing targets at concentration c is

$$\hat{S}_c(t) = \lim_{|\Gamma|\to\infty} \left[\int_{\Gamma} S(t;\mathbf{x}_0) d^3\mathbf{x}_0 / |\Gamma| \right]^{|\Gamma| c}, \tag{6}$$

which can be rewritten as

$$\hat{S}_c(t) = \exp\left(-c \int_{\Gamma} [1 - S(t;\mathbf{x}_0)] d^3\mathbf{x}_0 \right). \tag{7}$$

Hence Eqs. (4) and (7) are two expressions for the spatially averaged survival probability of a walker amongst a group of targets, and both are written in terms of $S(t;\mathbf{x}_0)$, which it remains to determine.

A. Describing the random walk

Recall that $S(t;\mathbf{x}_0)$ is the survival probability of a walker given that there is a target located at $\mathbf{x}_0$. This is the distribution of encounter times between the walker and the single target. By a change of coordinates we may equivalently take the target to be at the origin, and then $\mathbf{x}_0$ is the initial position of the walker. The latter approach proves more convenient and is used henceforth. The model geometry is shown in Fig. 2. We model the target as a stationary sphere with an "effective radius" r_d to account for its irregular shape and the rapid motion of its dendrites. The walker is modeled as a sphere of radius r_t which moves according to a "velocity-jump" process [21]. We will use "reaction" to mean the collision of a walker with a target, which occurs when the center of the

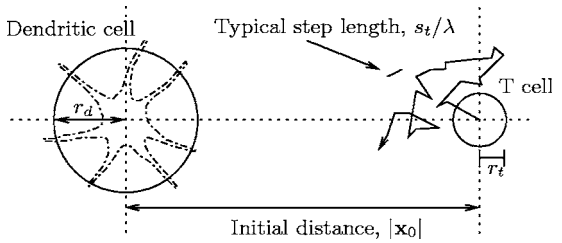

FIG. 2. The model geometry.

walker is a distance $a=r_d+r_t$ from the center of the target; a is henceforth termed the "reaction radius." The constant-speed version of the velocity-jump equation given by Othmer *et al.* [21] is

$$\frac{\partial q}{\partial t} + s_t \nabla \cdot (\mathbf{\Omega} q) = -\lambda q + \lambda \int T(\mathbf{\Omega}, \mathbf{\Omega}') q(\mathbf{x}, \mathbf{\Omega}', t; \mathbf{x}_0) d^2\mathbf{\Omega}', \tag{8}$$

where s_t is the speed of the walker, $\mathbf{\Omega}$ is its direction ($|\mathbf{\Omega}|=1$), and $T(\mathbf{\Omega}, \mathbf{\Omega}')$ is the probability that a re-orientation will change the walker's direction from $\mathbf{\Omega}'$ to $\mathbf{\Omega}$. The dependent variable $q(\mathbf{x}, \mathbf{\Omega}, t; \mathbf{x}_0)$ is a joint probability density function (PDF) for the position $\mathbf{x}$ and the direction $\mathbf{\Omega}$ of the walker at time t. Equation (8) is the limit over many realizations of a discrete process in which the cell moves at constant speed in straight-line segments. The interval durations are chosen from an exponential distribution with mean $1/\lambda$. In between intervals the cell re-orients itself randomly according to the turning kernel T.

We first consider the simple case in which the re-orientations are isotropic (this assumption is discussed later in Sec. IV). The assumption neglects any correlation between the pre- and post-turn directions and corresponds in three dimensions to choosing

$$T(\mathbf{\Omega}, \mathbf{\Omega}') = \frac{1}{4\pi}. \tag{9}$$

Thus, with isotropic turning, the governing equation (8) becomes

$$\frac{\partial q}{\partial t} + s_t \nabla \cdot (\mathbf{\Omega} q) = -\lambda q + \frac{\lambda p}{4\pi}, \tag{10}$$

where

$$p(\mathbf{x}, t; \mathbf{x}_0) = \int q(\mathbf{x}, \mathbf{\Omega}, t; \mathbf{x}_0) d^2\mathbf{\Omega} \tag{11}$$

is the PDF for the position of the walker.

The survival probability is related to the position of the walker in the sense that a surviving walker is one whose position has not come within a distance a of the center of the target by time t. We can regard an encounter as a process which removes a walker from the domain, thus $S(t; \mathbf{x}_0)$ is simply the probability that the walker remains within the domain at time t. Hence

$$S(t; \mathbf{x}_0) = \int_\Gamma p(\mathbf{x}, t; \mathbf{x}_0) d^3\mathbf{x}, \tag{12}$$

where Γ is the exterior to the sphere of radius a at the origin.

In the literature of diffusion-limited reactions the evolution of the position PDF, $p(\mathbf{x}, t; \mathbf{x}_0)$, is governed by a diffusion equation. While a random walk such as that described for the walker may resemble diffusion on a sufficiently long time scale, we use as our starting point Eq. (10) in order to capture behavior at intermediate times.

Since we are only interested in the survival probability of a walker, the functions $p(\mathbf{x}, t; \mathbf{x}_0)$ and $q(\mathbf{x}, \mathbf{\Omega}, t; \mathbf{x}_0)$ contain more information about the walker than we require. Our approach is thus to derive an expression for $S(t; \mathbf{x}_0)$ from Eq. (10) by integrating to remove unnecessary information.

B. Moment closure

Equation (10) can be integrated with respect to $\mathbf{\Omega}$ to give

$$\frac{\partial p}{\partial t} + s_t \nabla \cdot \mathbf{J} = 0, \tag{13}$$

where

$$\mathbf{J} = \int q \mathbf{\Omega} d^2\mathbf{\Omega}, \tag{14}$$

and $s_t\mathbf{J}$ is the probability flux.

Equation (13) is not closed for p because the flux $\mathbf{J}$ is unknown. An expression for $\mathbf{J}$ can be obtained from multiplying Eq. (10) by $\mathbf{\Omega}$ then integrating over $\mathbf{\Omega}$, hence

$$\frac{\partial \mathbf{J}}{\partial t} + s_t \nabla \cdot \int q \mathbf{\Omega}\mathbf{\Omega} d^2\mathbf{\Omega} = -\lambda \mathbf{J}. \tag{15}$$

This equation for $\mathbf{J}$ is written in terms of the second velocity moment of q (i.e., $\int q\mathbf{\Omega}\mathbf{\Omega} d^2\mathbf{\Omega}$) which is unknown. In general, multiplying Eq. (10) by $\mathbf{\Omega}^n$ and integrating over $\mathbf{\Omega}$ relates the nth and $(n+1)$th velocity moments, and so the number of unknowns exceeds the number of equations. Hence further assumptions are required to close the system.

Following (for example) Bearon and Pedley [25] we consider the behavior on length and time scales much greater than those of the individual random walk steps; this is the appropriate regime because a T cell will typically make a large number of steps before it encounters an DC. Referring to Fig. 2 and recalling that $a=r_d+r_t$, the distance a walker must travel to encounter a target is $|\mathbf{x}_0|-a$. Since the mean length of an individual step is s_t/λ, we introduce the dimensionless parameter

$$\varepsilon = \frac{s_t/\lambda}{|\mathbf{x}_0| - a}, \tag{16}$$

which we assume to be small ($\varepsilon \ll 1$). We nondimensionalize $\mathbf{x}$ on the mean step length and rescale on ε so that the initial walker-target separation is $O(1)$, hence

$$\mathbf{x} = \frac{s_t}{\lambda\varepsilon}\tilde{\mathbf{x}}, \tag{17}$$

where the tildes are used to denote dimensionless variables. We similarly nondimensionalize t on the mean step time and use the diffusion scaling $t \sim |\mathbf{x}|^2$ so that

$$t = \frac{1}{\lambda\varepsilon^2}\tilde{t}. \tag{18}$$

The dependent variables are nondimensionalized by

$$(p, q, \mathbf{J}) = \left(\frac{\varepsilon\lambda}{s_t}\right)^3 (\tilde{p}, \tilde{q}, \tilde{\mathbf{J}}). \tag{19}$$

Dropping tildes for convenience, the governing equations (10), (13), and (15) become

$$\varepsilon^2\frac{\partial q}{\partial t} + \varepsilon\boldsymbol{\nabla}\cdot(q\boldsymbol{\Omega}) = -q + \frac{p}{4\pi}, \tag{20}$$

$$\varepsilon^2\frac{\partial p}{\partial t} + \varepsilon\boldsymbol{\nabla}\cdot\mathbf{J} = 0, \tag{21}$$

$$\varepsilon^2\frac{\partial \mathbf{J}}{\partial t} + \varepsilon\boldsymbol{\nabla}\cdot\int q\boldsymbol{\Omega}\boldsymbol{\Omega}d^2\boldsymbol{\Omega} = -\mathbf{J}. \tag{22}$$

Expanding the dependent variables in powers of ε (i.e., $p = p_0 + \varepsilon p_1 + \varepsilon^2 p_2 + \cdots$, with similar expansions for q and $\mathbf{J}$) and using the identities in Appendix A leads to

$$\begin{aligned} q &= \frac{1}{4\pi}\left[p_0 + \varepsilon(p_1 - \boldsymbol{\Omega}\cdot\boldsymbol{\nabla}p_0) + \varepsilon^2\left(p_2 - \frac{\partial p_0}{\partial t} - \boldsymbol{\Omega}\cdot\boldsymbol{\nabla}(p_1 - \boldsymbol{\Omega}\cdot\boldsymbol{\nabla}p_0)\right)\right] + O(\varepsilon^3) \\ &= \frac{1}{4\pi}\left[p - \varepsilon\boldsymbol{\Omega}\cdot\boldsymbol{\nabla}p + \varepsilon^2\left(-\frac{\partial p}{\partial t} + (\boldsymbol{\Omega}\cdot\boldsymbol{\nabla})^2 p\right)\right] + O(\varepsilon^3), \end{aligned} \tag{23}$$

$$\begin{aligned} \mathbf{J} &= -\varepsilon\frac{1}{3}\boldsymbol{\nabla}p_0 - \varepsilon^2\frac{1}{3}\boldsymbol{\nabla}p_1 + \varepsilon^3\left(\frac{2}{3}\frac{\partial}{\partial t}\boldsymbol{\nabla}p_0 - \frac{1}{3}\boldsymbol{\nabla}p_2 - \frac{1}{5}\boldsymbol{\nabla}\nabla^2 p_0\right) \\ &\quad + O(\varepsilon^4) \\ &= -\varepsilon\frac{1}{3}\boldsymbol{\nabla}p + \varepsilon^3\left(\frac{2}{3}\frac{\partial}{\partial t}\boldsymbol{\nabla}p - \frac{1}{5}\boldsymbol{\nabla}\nabla^2 p\right) + O(\varepsilon^4), \end{aligned} \tag{24}$$

where the expressions are written in terms of the composite asymptotic approximation for p, which contains information about p at each order. Substituting $\mathbf{J}$ from Eq. (24) into Eq. (21) gives

$$\frac{\partial p}{\partial t} = \frac{1}{3}\nabla^2 p - \varepsilon^2\left(\frac{2}{3}\frac{\partial}{\partial t}\nabla^2 p - \frac{1}{5}\nabla^4 p\right) + O(\varepsilon^3) \tag{25}$$

in $r \geq b$, where $b = \varepsilon\lambda a/s_t$. Hence p satisfies

$$\frac{\varepsilon^2}{5}\frac{\partial^2 p}{\partial t^2} + \frac{\partial p}{\partial t} = \frac{1}{3}\nabla^2 p + O(\varepsilon^3), \tag{26}$$

which is the telegrapher's equation. It is also necessary to determine the conditions for p on an absorbing boundary.

C. Boundary condition on a target

We consider the surface of a target to be an "absorbing" boundary, so that a walker which touches the target is removed from the domain. The formal condition on q is

$$q(\mathbf{x}, \boldsymbol{\Omega}, t; \mathbf{x}_0)\big|_{\partial\Gamma_{\text{abs}}} = 0 \quad \text{for } \boldsymbol{\Omega} \text{ such that } \boldsymbol{\Omega}\cdot\mathbf{n} > 0, \tag{27}$$

where $\partial\Gamma_{\text{abs}}$ is the surface of the target and $\mathbf{n}$ is a unit vector normal to the surface, pointing into the domain. However, to solve Eq. (26) we must determine a condition on p. We do so by imposing the weaker condition that the local flux of inbound walkers is zero:

$$J_{\text{in}}(\mathbf{x}, t)\big|_{\partial\Gamma_{\text{abs}}} = \mathbf{n}\cdot\int_{\text{in}} q\big|_{\partial\Gamma_{\text{abs}}}\boldsymbol{\Omega}d^2\boldsymbol{\Omega} = 0, \tag{28}$$

where the integral is performed over the hemisphere of inwardly pointing directions. Substituting q from Eq. (23) and using the integral identities given in Appendix A leads to the following condition on p:

$$\left[p - \varepsilon\frac{2}{3}\mathbf{n}\cdot\boldsymbol{\nabla}p + \varepsilon^2\left(-\frac{1}{12}\nabla^2 p + \frac{1}{4}(\mathbf{n}\cdot\boldsymbol{\nabla})^2 p\right)\right]\Bigg|_{\partial\Gamma_{\text{abs}}} + O(\varepsilon^3) = 0. \tag{29}$$

D. Formulation in terms of the survival distribution

Tachiya [20] exploits the property

$$p(\mathbf{x}, t; \mathbf{x}_0) = p(\mathbf{x}_0, t; \mathbf{x}) \tag{30}$$

for any function p which solves the diffusion equation plus suitable boundary and initial conditions. In Appendix B we show that Eq. (30) also holds for solutions of Eqs. (26) and

(29). Using Eq. (30) allows the governing equation to be written with the spatial arguments reversed, resulting in the so-called "adjoint" or "backward" equation,

$$\frac{\varepsilon^2}{5}\frac{\partial^2 p}{\partial t^2}+\frac{\partial p}{\partial t}=\frac{1}{3}\nabla_0^2 p+O(\varepsilon^3), \tag{31}$$

where ∇_0^2 operates on the initial position $\mathbf{x}_0$. Recall that we wish to solve for the survival probability S and that p contains more information than required. Using the definition of $S(t;\mathbf{x}_0)$ from Eq. (12), Eq. (31) can be integrated with respect to $\mathbf{x}$ to give

$$\frac{\varepsilon^2}{5}\frac{\partial^2 S}{\partial t^2}+\frac{\partial S}{\partial t}=\frac{1}{3}\nabla_0^2 S+O(\varepsilon^3). \tag{32}$$

Provided the initial walker-target separation is sufficiently large that the exponentially small absorption of walkers at small times can be neglected, then the initial condition on S is

$$S|_{t=0}=\int p|_{t=0}d^3\mathbf{x}=1, \tag{33}$$

which is independent of the initial position $\mathbf{x}_0$. Since the boundary conditions are spherically symmetric, so must be the solution, $S=S(t;|\mathbf{x}_0|)$. Hence the governing equation for S is

$$\frac{\varepsilon^2}{5}\frac{\partial^2 S}{\partial t^2}+\frac{\partial S}{\partial t}=\frac{1}{3r^2}\frac{\partial}{\partial r}\left(r^2\frac{\partial S}{\partial r}\right), \tag{34}$$

where $r=|\mathbf{x}_0|$ is the distance from the walker's initial position to the center of the target.

The boundary conditions on S can be determined in the same way, using the reciprocal relationship (30) to write the boundary conditions on p with the arguments reversed and then integrating over $\mathbf{x}$. Following this procedure we obtain

$$\left\{S-\varepsilon\frac{2}{3}\frac{\partial S}{\partial r}+\varepsilon^2\left[\frac{1}{4}\frac{\partial^2 S}{\partial r^2}-\frac{1}{12r^2}\frac{\partial}{\partial r}\left(r^2\frac{\partial S}{\partial r}\right)\right]\right\}\Bigg|_{r=b}=0, \tag{35}$$

$$\lim_{r\to\infty} S=1. \tag{36}$$

III. RESULTS

A. Solution for the single-target problem

To solve Eqs. (34)–(36) we seek a solution

$$S=S_0+\varepsilon S_1+\varepsilon^2 S_2+\cdots. \tag{37}$$

The leading-order problem is then

$$\frac{\partial S_0}{\partial t}=\frac{1}{3r^2}\frac{\partial}{\partial r}\left(r^2\frac{\partial S_0}{\partial r}\right);\quad S_0|_{t=0}=1,\quad S_0|_{r=b}=0,\quad \lim_{r\to\infty} S_0=1, \tag{38}$$

which is the Smoluchowski diffusion problem. The solution is

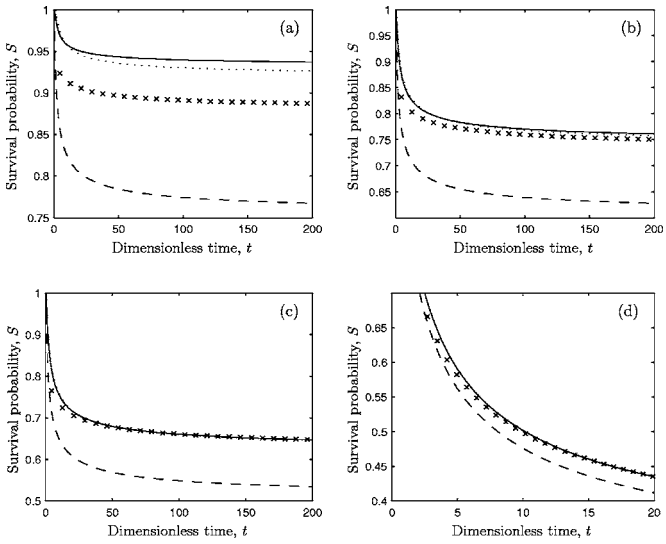

FIG. 3. Plots of the survival distribution (37) for a variety of target radii and initial positions. The solution (37) is plotted to leading order (dashed line), to $O(\varepsilon)$ (dotted line), and to $O(\varepsilon^2)$ (solid line). Shown are plots for (a) $\varepsilon=1/3$, $b=1/3$, $r=|\mathbf{x}_0|=4/3$, (b) $\varepsilon=1/3$, $b=2/3$, $r=5/3$, (c) $\varepsilon=1/3$, $b=1$, $r=2$, and (d) $\varepsilon=1/10$, $b=3$, $r=4$. The crosses in each graph show the survival distribution calculated from 7×10^4 Monte Carlo trials. The analytical solution becomes increasingly inaccurate as the ratio of the reaction radius to the step length, $a\lambda/s_t=b/\varepsilon$, decreases.

$$S_0=1-\frac{b}{r}\operatorname{erfc}(\eta),\quad \text{where } \eta=\frac{\sqrt{3}}{2}\frac{(r-b)}{\sqrt{t}}. \tag{39}$$

The solutions at the next two orders are

$$S_1=\frac{2}{3r}\left(\frac{\sqrt{3}b}{\sqrt{\pi t}}\exp(-\eta^2)+\operatorname{erfc}(\eta)\right), \tag{40}$$

$$S_2=\frac{1}{r}\left[\exp(-\eta^2)\left(\frac{b\eta^3}{5\sqrt{\pi t}}-\frac{7\sqrt{3}}{18\sqrt{\pi t}}\right)+\frac{1}{18b}\operatorname{erfc}(\eta)\right]. \tag{41}$$

These solutions are plotted in Fig. 3. Note that retaining the $O(\varepsilon)$ term increases the survival probability of the random walker. The $O(\varepsilon^2)$ correction is small; S_2 is negative for small times and positive for large times.

B. Solution by Monte Carlo simulation

To test the validity of the analytical results we performed Monte Carlo simulations to calculate the survival probability of a walker in the presence of either a single target or a uniform distribution of targets. The simulated system implements the same assumptions as the mathematical model: the walker moves at constant velocity for intervals whose lengths are drawn from an exponential distribution, between which the walker reorientiates isotropically. The simulation runs until the separation between the walker and a target center is equal to the reaction radius a, at which point the survival time is recorded. After performing a large number of

realizations, the survival probability $S(t;\mathbf{x}_0)$ is calculated as the proportion of cells whose survival time exceeds t.

Figure 3 shows a comparison between the simulation results and the analytical solution for a walker in the presence of a single target. The solutions agree very well in (c) and (d) when the step length s_t/λ is smaller than the reaction radius a, but the analytical solution breaks down in (a) and (b) when the step length and reaction radius are of comparable size. To understand this, note that in deriving the governing equation and boundary conditions (34)–(36) we have expanded in powers of ε. It follows then that to subsequently apply a boundary condition on $r=b$ we require $b=\varepsilon\lambda a/s_t \gg \varepsilon$, i.e., $a \gg s_t/\lambda$, hence the target must be larger than the step length. Physically, the breakdown occurs because in the expansion (23) q is isotropic to leading order over $O(1)$ lengths. Since q depends strongly on direction $\mathbf{\Omega}$ on opposite sides of the target, applying the boundary condition (29) for a small target violates the isotropy of Eq. (23).

C. Solution for multiple targets

The solution for $S(t;\mathbf{x}_0)$ can be used with either Eq. (4) or Eq. (7) to calculate the survival probability for a walker in the presence of numerous targets. Recall that Eq. (4) is appropriate to use when the number of targets N is small and Eq. (7) is more convenient when N is large. However, if Γ is finite then Eq. (7) is valid only at early times when the effects from walkers which escape Γ can be neglected.

Here we calculate $\hat{S}_c(t)$ using Eq. (7). The calculation requires an integral with respect to $\mathbf{x}_0$ and (because ε depends on $\mathbf{x}_0$) it is convenient to revert to dimensional variables. Thus the leading-order integral is

$$\int_\Gamma [1 - S_0(t;\mathbf{x}_0)] d^3\mathbf{x}_0 = 4a\sqrt{\pi\sigma}(2a\sqrt{\pi} + \sqrt{\pi\sigma t}), \quad (42)$$

where $\sigma = s_t^2/(3\lambda)$. At next order,

$$\int_\Gamma \varepsilon S_1(t;\mathbf{x}_0) d^3\mathbf{x}_0 = \frac{8\sqrt{\pi}\sigma}{s_t}(\sqrt{\pi}a^2 + 4a\sqrt{\sigma t} + \sqrt{\pi}\sigma t), \quad (43)$$

and finally at $O(\varepsilon^2)$

$$\int_\Gamma \varepsilon^2 S_2(t;\mathbf{x}_0) d^3\mathbf{x}_0 = \frac{2\sqrt{\pi}\sigma^{3/2}}{5s_t^2}\left(\frac{6a^2}{\sqrt{t}} - 26a\sqrt{\pi\sigma} - 60\sqrt{t}\sigma + \frac{5\sqrt{\pi}\sigma^{3/2}t}{a}\right). \quad (44)$$

The results are shown in Fig. 4. Equation (44) diverges as $t \to 0$; however, solutions of Eq. (32) are valid only for $t \gg \varepsilon^2$. The initial transient behavior cannot be described without formulating and solving the early-time problem.

D. Solution with biological parameters

The biological parameters related to cell size and motility are summarized in Table I. The ratio between the reaction radius and step length is $(r_d + r_t)/(s_t/\lambda) \approx 1.14$. Because this ratio is only slightly greater than unity, the regime is similar to the regime of Fig. 3(a) in which the analysis overpredicts the survival probability for the single-target problem. This overprediction is also reflected in the solution for the multiple-target problem, shown in Fig. 4.

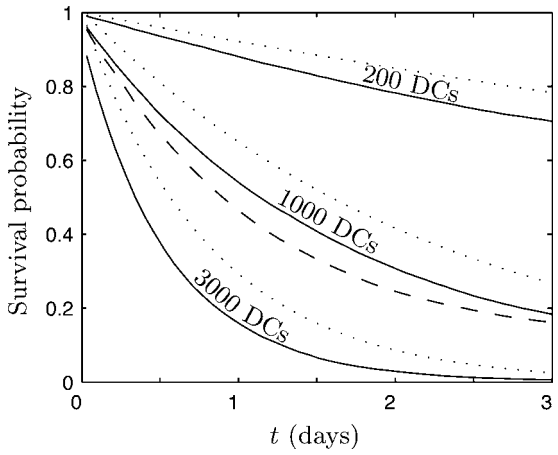

FIG. 4. The survival probability for a single cell within a lymph node; with reaction radius $a=25$ μm, and the DC concentration calculated supposing there are (i) 200, (ii) 1000, and (iii) 3000 DCs uniformly distributed within a spherical paracortex of radius 2 mm. The solid lines are calculated from 2×10^4 Monte Carlo trials, assuming the T cell re-orients isotropically; the dotted lines show the analytical solution from equations (7) and (42)–(44). The dashed line is the Monte Carlo solution (for 1000 targets, from 2×10^4 trials) for a walker which re-orients according to the empirical turning distribution measured by Mempel *et al.* [9] (shown as dots in Fig. 5).

Table I does not include the concentration of DCs within the lymph node because this parameter has not been accurately measured. Bousso and Robey [5] performed an experiment in which antigen-primed DCs were injected subcutaneously into mice and antigen-specific T cells were injected intravenously. They estimated that of the 10^6 injected DCs, around 10^3–10^4 DCs reached the draining lymph node. Although the number of antigen-bearing DCs within the lymph node following adoptive transfer is not necessarily representative of the number of DCs in a lymph node after a natural infection, Bousso and Robey's estimate is the best available. The solution for $S_c(t)$ for various numbers of DCs is shown in Fig. 4.

Bousso and Robey [5] reported that around 50% of the transferred T cells were engaged with DCs 20 h after injection. Assuming the paracortex has a radius of 2 mm then our results, shown in Fig. 4, are consistent with Bousso and Robey's observations provided the number of DCs is within their estimated range.

Bousso and Robey [5] also estimated that a single DC can scan as many as 500 T cells per hour. From this observation they concluded that 200 DCs would be sufficient to detect a naive antigen-specific T cell at a frequency of 1 in 10^5 within 1 h. This calculation assumes that surveillance of T cells by DCs is optimal; however, according to the random-walk model, the surveillance is stochastic and transport-limited. Our results show that the probability that 200 uniformly dis-

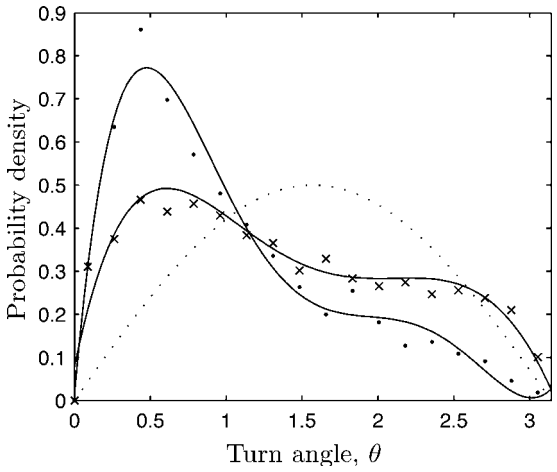

FIG. 5. A graph of data taken from Mempel *et al.* [9] showing the turning distributions of T cells within the paracortex of a lymph node. The two data sets correspond to the T cells turning in the presence (dots) and absence (crosses) of peptide-bearing antigen-presenting cells. The two solid lines are fifth-order polynomial fits, and the dotted line is the PDF which characterizes the distribution of the turning angle Θ for an isotropic random walk, $\text{Prob}\{\theta < \Theta < \theta + d\theta\} = \frac{1}{2} \sin\theta d\theta$.

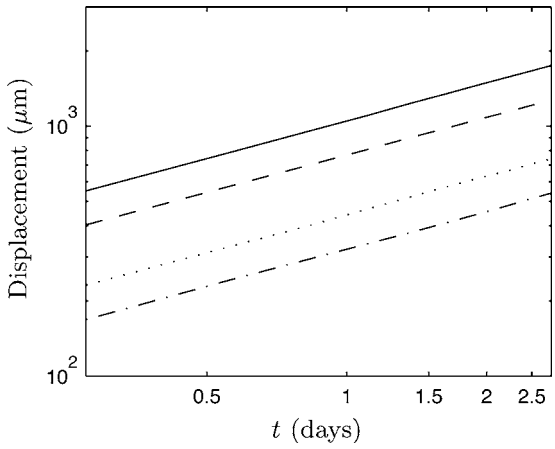

FIG. 6. The mean (dash) and standard deviation (dot-dash) of displacements for a random walker which turn isotropically, compared with the mean (solid) and standard deviation (dot) of displacements for a random walker which turns according to the empirical distribution from Ref. [9] (shown as dots in Fig. 5). Each line is calculated from 2×10^4 trials, using parameter values appropriate for a T cell: $s_t = 11\ \mu\text{m min}^{-1}$, $\lambda = 1/2\ \text{min}^{-1}$. The mean and standard deviation are larger for the persistent walk than for the isotropic walk.

tributed DCs will detect any single T cell within 3 days is only $\approx 30\%$. To ensure with probability $>50\%$ that a T cell in a paracortex of radius 2 mm is activated within 24 h, the required number of DCs is ≈ 1200; this is a density of ≈ 35 cells mm^{-3}. The transport process by which T cells and DCs interact means that far more DCs are required for effective surveillance than Bousso and Robey's estimate.

E. Effect of anisotropic re-orientation

So far we have assumed that the random walker re-orients itself isotropically each time it turns. A distribution which characterizes T-cell turning has been measured experimentally by Mempel *et al.* [9]. Figure 5 shows the contrast between the observed turning distribution [9] and the isotropic distribution. The observed distribution is skewed towards a small turning angle which indicates that a T cell tends to choose a new direction similar to its pre-turn direction, a property termed persistence. Figure 6 contrasts the displacement of isotropic and anisotropic walkers (assuming no targets), calculated using Monte Carlo simulations and biological parameters. The mean and standard deviation of the displacement are notably larger for the more persistent walker.

To understand how anisotropic turning affects the survival distribution for a T cell moving amongst target DCs, we ran simulations in which the walker turned according to the distribution shown as dots in Fig. 5. The solution, plotted as the dashed line in Fig. 4, shows that the increased persistence reduces the survival probability at small times when compared with an isotropic walker, though the effect is small. However, the persistent walker's asymptotic survival probability is larger than the isotropic walker's (not shown on the graph) because the persistent walker escapes Γ with a higher probability.

IV. DISCUSSION

The recent experimental effort to characterize migration of immune cells within the lymph node has led to a greater understanding of how adaptive immunity is generated. In this paper we have modeled the movement of T cells as a random walk and, by using parameters reported in the experimental literature, we have provided a quantitative analysis of the time it takes for an antigen-specific T cell to encounter an antigen-bearing DC.

Comparison with Monte Carlo simulations shows that the analytical solution for the survival distribution overestimates the real solution. This difference occurs because the radius of a dendritic cell is not much larger than the length of a typical T cell step. The analytical solution is reasonable, however, and shows explicitly the dependence of the solution on the model parameters.

We have modeled the DCs as uniformly distributed, stationary spheres and the T cell as a fixed-speed random walker which re-orients randomly between exponentially distributed intervals. Further assuming that the re-orientations were isotropic made the problem amenable to analysis and allowed the solution to be written so that its dependence on biological parameters is explicit. Taking these assumptions in turn, let us consider their validity and how they affect the solution.

Studies using two-photon microscopy show that some DCs are motile, although there is disagreement regarding DC speed: Miller *et al.* [7] report a mean of $2-3\ \mu\text{m s}^{-1}$, whereas Bousso and Robey [5] observed a mean of $5-6\ \mu\text{m s}^{-1}$. The discrepancy may be due to differences in behavior between antigen-primed and unprimed DCs. Also, Bousso and Robey measure the position of the center of mass of the DC, which changes very rapidly due to shape changes caused by motion of the dendrites. Thus the mean

speed may be deceptively large with a strong correlation between the directions of subsequent steps. In other words, the position of the center of mass may oscillate rapidly, but the net displacement over a number of steps may be small. The plots in Refs. [5,9] of individual DC paths support this idea. Hence to model accurately the motion of a DC one must bear in mind the correlations between steps.

We have also assumed that the distribution of DCs is uniform. Mempel *et al.* [9] observed that DCs may strategically position themselves near to the high-endothelial venules from which T cells emerge into the lymph node, thus targets may be clustered close to the initial position of the walker. A nonuniform target distribution can be incorporated into the model by replacing Eq. (3) with

$$\hat{S}(t) = \int_{\Gamma} u(\mathbf{x}_0) S(t;\mathbf{x}_0) d^3\mathbf{x}_0, \tag{45}$$

where $u(\mathbf{x}_0)$ is defined such that $\int_\gamma u(\mathbf{x}_0) d^3\mathbf{x}_0$ is the probability that any given target is centered in the arbitrary volume γ. The uniform distribution, $u(\mathbf{x}_0)=1/|\Gamma|$, which we have used throughout, provides an upper bound on the survival probability of a walker whose targets are strategically clustered.

We have modeled the T cell as a constant-speed random walker. The more general velocity-jump equation of Othmer *et al.* [21] can be used for a variable speed walker; however, the data currently available are not sufficient to determine the distribution of T cell speeds. Likewise, the assumption that the step intervals are exponentially distributed can be replaced once the step length distribution is accurately characterized experimentally.

In the analysis we assumed that a T cell re-orients itself isotropically when it turns. A more accurate model incorporates the turning distribution reported by Mempel *et al.* [9]. The persistence can be quantified by calculating the mean of the cosine of the turning angle ϕ [26]. For an isotropic walker $\phi=0$, whereas for a perfectly persistent walker $\phi=1$. For the data from Ref. [9] we calculate $\phi=0.47$ in the absence of peptide-bearing DCs and $\phi=0.17$ when DCs are present. This is evidence that T-cell motility patterns are altered within an antigen-challenged lymph node. It remains unclear whether a T cell is able to detect that peptide-bearing DCs are nearby and adapt its searching strategy, or whether the different migratory behavior is due to altered physiological conditions within a challenged lymph node.

Considering a nonisotropic walker analytically corresponds to choosing a turning kernel, $T(\mathbf{\Omega},\mathbf{\Omega}')$, which is a function of the angle between the pre- and post-turn directions. With nonconstant T it is less straightforward to derive an equation for p because Eq. (8) remains an integral-differential equation. Techniques for doing so have been discussed by Hillen and Othmer [27]. Figure 4 shows that the anisotropic turning distribution has a small effect on the survival distribution, and incorporating anisotropic turning into the analysis is probably not warranted until other aspects of the model are refined.

Castellino *et al.* [10] have recently suggested that DCs actively attract T cells by secreting chemokines. Chemotaxis can be incorporated in the model once the biological mechanism is established; it is currently not known whether T cells bias their re-orientations towards a target, whether T cells suppress their turning rate when moving in a preferential direction, or whether they use another mechanism. A potential disadvantage of chemotaxis is that T cells could accumulate around DCs, leading to congestion which inhibits surveillance. A computational model which considers competition for occupancy would be required to resolve this complicated question.

In conclusion, we have presented a model for the movement of T cells amongst dendritic cells. We have calculated a distribution which characterizes the time taken for an individual T cell to encounter an antigen-presenting DC, and Eqs. (4), (7), and (42)–(44) make clear the dependence of the survival time on physical parameters. Our results may be used to determine rate coefficients for larger-scale differential-equation models of the immune response.

ACKNOWLEDGMENTS

This work was funded by the Engineering and Physical Sciences Research Council (EPSRC) and WALTHAM Centre for Pet Nutrition.

APPENDIX A: INTEGRAL IDENTITIES IN THREE DIMENSIONS

The following identities are used to calculate Eqs. (23) and (24):

$$\int \Omega_i d^2\mathbf{\Omega} = \int \Omega_i \Omega_j \Omega_k d^2\mathbf{\Omega} = 0, \tag{A1}$$

$$\int \Omega_i \Omega_j d^2\mathbf{\Omega} = \frac{4\pi}{3}\delta_{ij}, \tag{A2}$$

$$\int \Omega_i \Omega_j \Omega_k \Omega_m d^2\mathbf{\Omega} = \frac{4\pi}{15} I_{ijkm}, \tag{A3}$$

where δ_{ij} is the Kronecker delta and $I_{ijkm}=\delta_{ij}\delta_{km}+\delta_{ik}\delta_{jm}+\delta_{im}\delta_{jk}$. The corresponding identities for integrals over the unit hemisphere, used to calculate Eq. (29), are

$$\int \Omega_i d^2\mathbf{\Omega} = \pi n_i, \tag{A4}$$

$$\int \Omega_i \Omega_j d^2\mathbf{\Omega} = \frac{2\pi}{3}\delta_{ij}, \tag{A5}$$

$$\int \Omega_i \Omega_j \Omega_k d^2\mathbf{\Omega} = \frac{\pi}{4}(n_m I_{ijkm} - n_i n_j n_k), \tag{A6}$$

where $\mathbf{n}$ is the normal to the flat side of the hemisphere, pointing into the hemisphere.

APPENDIX B: PROOF OF THE RECIPROCAL PROPERTY, $p(\mathbf{x},t;\mathbf{x}_0)=p(\mathbf{x}_0,t;\mathbf{x})$

We now show that $p(\mathbf{x},t;\mathbf{x}_0)$ is reciprocal in its spatial arguments when p solves the system

$$\varepsilon^2\frac{\partial^2 p}{\partial t^2}+\frac{\partial p}{\partial t}=\nabla^2 p, \tag{B1}$$

$$\left[p+\varepsilon\beta\frac{\partial p}{\partial n}+\varepsilon^2\left(\gamma\frac{\partial^2 p}{\partial n^2}+\zeta\nabla^2 p\right)\right]\Bigg|_{\partial\Gamma}=0, \tag{B2}$$

subject to an initial condition $p|_{t=0}$, where β, γ, and ζ are constants and $\partial\Gamma$ is an absorbing boundary. Note we require only a single initial condition to solve perturbatively at large times.

It is sufficient and simpler to show that the Laplace transform of p is reciprocal in its spatial arguments, i.e., $\bar{p}(\mathbf{x},s;\mathbf{x}_0)=\bar{p}(\mathbf{x}_0,s;\mathbf{x})$, where the overbar represents a Laplace transform with respect to t. Hence Laplace transforming the governing equation, boundary, and initial condition for p gives

$$\mathcal{L}\bar{p}\equiv(\nabla^2-s-\varepsilon^2 s^2)\bar{p}(\mathbf{x},s;\mathbf{x}_0) = -p(\mathbf{x},t;\mathbf{x}_0)\Big|_{t=0}(s\varepsilon^2+1)-\varepsilon^2\frac{\partial p}{\partial t}(\mathbf{x},t;\mathbf{x}_0)\Big|_{t=0}, \tag{B3}$$

$$0=\left[\bar{p}+\varepsilon\beta\frac{\partial\bar{p}}{\partial n}+\varepsilon^2\left(\gamma\frac{\partial^2\bar{p}}{\partial n^2}+\zeta\nabla^2\bar{p}\right)\right]\Bigg|_{\partial\Gamma}. \tag{B4}$$

Noting that the operator $\mathcal{L}$ is self-adjoint, we consider the integral

$$\int_\Gamma(\bar{v}\mathcal{L}\bar{p}-\bar{p}\mathcal{L}\bar{v})d^3\mathbf{x}, \tag{B5}$$

where $\bar{v}=\bar{v}(\mathbf{x},s)$ is a yet-unspecified function. This may be re-written

$$\int_\Gamma(\bar{v}\nabla^2\bar{p}-\bar{p}\nabla^2\bar{v})d^3\mathbf{x} \tag{B6}$$

$$=\int_\Gamma\boldsymbol{\nabla}\cdot(\bar{v}\boldsymbol{\nabla}\bar{p}-\bar{p}\boldsymbol{\nabla}\bar{v})d^3\mathbf{x} \tag{B7}$$

$$=\int_{\partial\Gamma}\left(\bar{v}\frac{\partial\bar{p}}{\partial n}-\bar{p}\frac{\partial\bar{v}}{\partial n}\right)d^2\mathbf{x} \tag{B8}$$

upon applying the divergence theorem. We now suppose that $\bar{v}$ solves

$$\mathcal{L}\bar{v}\equiv(\nabla^2-s-\varepsilon^2 s^2)\bar{v}(\mathbf{x},s;\boldsymbol{\xi})=-v(\mathbf{x},t;\boldsymbol{\xi})\Big|_{t=0}(s\varepsilon^2+1) -\varepsilon^2\frac{\partial v}{\partial t}(\mathbf{x},t;\boldsymbol{\xi})\Big|_{t=0}, \tag{B9}$$

and satisfies the same boundary conditions as $\bar{p}$ (B4). We assume that $p|_{t\to 0}$ satisfies

$$\int_\Gamma F(\mathbf{x})\lim_{t\to 0}p(\mathbf{x},t;\mathbf{x}_0)d^3\mathbf{x}=F(\mathbf{x}_0)\int_\Gamma\lim_{t\to 0}p(\mathbf{x},t;\mathbf{x}_0)d^3\mathbf{x}=F(\mathbf{x}_0), \tag{B10}$$

for some function $F(\mathbf{x})$. Furthermore, by conservation of mass $\int p d^3\mathbf{x}=1$ for $t\geq 0$, so

$$\int_\Gamma\frac{\partial p}{\partial t}(\mathbf{x},t;\mathbf{x}_0)d^3\mathbf{x}=\frac{\partial}{\partial t}\int_\Gamma p(\mathbf{x},t;\mathbf{x}_0)d^3\mathbf{x}=0, \tag{B11}$$

because Γ is fixed. Hence, since $\partial p/\partial t$ is singular as $t\to 0$, we assume

$$\int_\Gamma F(\mathbf{x})\lim_{t\to 0}\frac{\partial p}{\partial t}d^3\mathbf{x}=F(\mathbf{x}_0)\int_\Gamma\lim_{t\to 0}\frac{\partial p}{\partial t}d^3\mathbf{x}=0. \tag{B12}$$

With Eqs. (B10) and (B12), and similar conditions for v, Eqs. (B5)–(B8) can be evaluated to leave

$$[\bar{p}(\boldsymbol{\xi},s;\mathbf{x}_0)-\bar{v}(\mathbf{x}_0,s;\boldsymbol{\xi})](s\varepsilon^2+1)=\int_{\partial\Gamma}\left(\bar{v}\frac{\partial\bar{p}}{\partial n}-\bar{p}\frac{\partial\bar{v}}{\partial n}\right)d^2\mathbf{x}. \tag{B13}$$

The integrand of the surface integral does not trivially vanish for absorbing boundaries. We proceed by exploiting the assumption that ε is small, expanding $\bar{p}$ and $\bar{v}$ as power series in ε, and then considering the relationship between $\bar{p}$ and $\bar{v}$ at each order.

The expansion of the boundary condition (B4) is (with overbars dropped)

$$p_0+\varepsilon\beta\left(p_1+\beta\frac{\partial p_0}{\partial n}\right)+\varepsilon^2\left(p_2+\beta\frac{\partial p_1}{\partial n}+\gamma\frac{\partial^2 p_0}{\partial n^2}+\zeta\nabla^2 p_0\right)=0, \tag{B14}$$

and $v_0,v_1,v_2,\ldots$ satisfy the same equations. From Eq. (B13) we then have

$$O(1):p_0(\boldsymbol{\xi},s;\mathbf{x}_0)-v_0(\mathbf{x}_0,s;\boldsymbol{\xi})=\int_{\partial\Gamma}\left(v_0\frac{\partial p_0}{\partial n}-p_0\frac{\partial v_0}{\partial n}\right)d^2\mathbf{x}=0, \tag{B15}$$

$$O(\varepsilon):p_1(\boldsymbol{\xi},s;\mathbf{x}_0)-v_1(\mathbf{x}_0,s;\boldsymbol{\xi})=\int_{\partial\Gamma}\left(v_1\frac{\partial p_0}{\partial n}-p_1\frac{\partial v_0}{\partial n}\right)d^2\mathbf{x} =\int_{\partial\Gamma}\frac{\partial p_0}{\partial n}\left(v_1+\beta\frac{\partial v_0}{\partial n}\right)d^2\mathbf{x}=0. \tag{B16}$$

Noting that p and v satisfy the same governing equation and boundary conditions we may write

$$p(\mathbf{y},s;\mathbf{y}_0)=v(\mathbf{y},s;\mathbf{y}_0), \tag{B17}$$

and by comparison with Eq. (B15) observe that

$$p_0(\mathbf{x},s;\mathbf{x}_0)=p_0(\mathbf{x}_0,s;\mathbf{x}), \tag{B18}$$

as required. The same reciprocal relationship holds for p_1 from Eq. (B16).

At $O(\varepsilon^2)$ the right hand side of Eq. (B13) is

$$\int_\Gamma \left(v_2\frac{\partial p_0}{\partial n} + v_1\frac{\partial p_1}{\partial n} + v_0\frac{\partial p_2}{\partial n} - p_2\frac{\partial v_0}{\partial n} - p_1\frac{\partial v_1}{\partial n} - p_0\frac{\partial v_2}{\partial n} \right) d^3\mathbf{x}$$
$$= \int_{\partial\Gamma} \left[v_0\frac{\partial p_2}{\partial n} - p_0\frac{\partial v_2}{\partial n} + \frac{\partial p_1}{\partial n}\left(v_1 + \beta\frac{\partial v_0}{\partial n} \right) \right.$$
$$- \frac{\partial v_1}{\partial n}\left(p_1 + \beta\frac{\partial p_0}{\partial n} \right) - \frac{\partial p_0}{\partial n}\left(\gamma\frac{\partial^2 v_0}{\partial n^2} + \zeta\nabla^2 v_0 \right)$$
$$\left. + \frac{\partial v_0}{\partial n}\left(\gamma\frac{\partial^2 p_0}{\partial n^2} + \zeta\nabla^2 p_0 \right) \right] d^2\mathbf{x}. \tag{B19}$$

Since $p_0=0$ on $\partial\Gamma$, we have $p_{0_t}=\nabla^2 p_0=0$ on $\partial\Gamma$ (and similarly for v_0). Thus a number of terms in the integrand vanish, leaving only

$$\gamma\int_{\partial\Gamma} \left(\frac{\partial v_0}{\partial n}\frac{\partial^2 p_0}{\partial n^2} - \frac{\partial p_0}{\partial n}\frac{\partial^2 v_0}{\partial n^2} \right) d^2\mathbf{x}, \tag{B20}$$

which it remains to show is zero. Suppose that the surface $\partial\Gamma$ is given in Cartesian coordinates by $f(x,y,z)=$const. Introducing transformed coordinates,

$$u_1 = u_1(x,y,z), \quad u_2 = u_2(x,y,z), \quad u_3 = u_3(x,y,z), \tag{B21}$$

we may write the position vector of some point $\mathbf{r}$ as

$$\mathbf{r} = \mathbf{r}(u_1,u_2,u_3). \tag{B22}$$

The unit vector ($|\mathbf{e}_1|=1$) normal to the surface $u_1=$const is

$$\mathbf{e}_1 = \frac{1}{h_1}\frac{\partial \mathbf{r}}{\partial u_1}, \quad \text{where } h_1 = \left| \frac{\partial \mathbf{r}}{\partial u_1} \right|, \tag{B23}$$

and the unit vectors $\mathbf{e}_2$ and $\mathbf{e}_3$ and scale factors h_2 and h_3 are defined similarly. We choose $u_1=f(x,y,z)$ so that $\mathbf{e}_1=\mathbf{n}$, and we choose u_2 and u_3 so that $\mathbf{e}_1\cdot\mathbf{e}_2=\mathbf{e}_1\cdot\mathbf{e}_3=\mathbf{e}_2\cdot\mathbf{e}_3=0$. The Laplacian in orthogonal curvilinear coordinates is [28]

$$\nabla^2 p_0 = \frac{1}{h_1h_2h_3}\left[\frac{\partial}{\partial u_1}\left(\frac{h_2h_3}{h_1}\frac{\partial p_0}{\partial u_1} \right) + \frac{\partial}{\partial u_2}\left(\frac{h_1h_3}{h_2}\frac{\partial p_0}{\partial u_2} \right) \right.$$
$$\left. + \frac{\partial}{\partial u_3}\left(\frac{h_1h_2}{h_3}\frac{\partial p_0}{\partial u_3} \right) \right], \tag{B24}$$

but since $p_0=\nabla^2 p_0=0$ on $\partial\Gamma$, and since $\mathbf{e}_2$ and $\mathbf{e}_3$ are tangential to $\partial\Gamma$, therefore $\partial p_0/\partial u_2=0=\partial p_0/\partial u_3=\partial^2 p_0/\partial u_2^2=\partial^2 p_0/\partial u_3^2$ on $\partial\Gamma$. Thus Eq. (B24) gives

$$\frac{\partial^2 p_0}{\partial n^2} = -\left(\frac{h_2h_3}{h_1} \right)^{-1}\frac{\partial}{\partial n}\left(\frac{h_2h_3}{h_1} \right)\frac{\partial p_0}{\partial n} \tag{B25}$$

on $\partial\Gamma$. A similar expression holds for v_0. Substituting these expressions into Eq. (B20) reveals that the integral is zero, as required.

At $O(\varepsilon^2)$ we therefore have

$$s[p_0(\boldsymbol{\xi},s;\mathbf{x}_0) - v_0(\mathbf{x}_0,s;\boldsymbol{\xi})] + p_2(\boldsymbol{\xi},s;\mathbf{x}_0) - v_2(\mathbf{x}_0,s;\boldsymbol{\xi}) = 0, \tag{B26}$$

and hence

$$p_2(\boldsymbol{\xi},s;\mathbf{x}_0) = v_2(\mathbf{x}_0,s;\boldsymbol{\xi}). \tag{B27}$$

Again, by comparing this with Eq. (B17) we see that p_2 is reciprocal in its spatial arguments and thus $p(\mathbf{x},s;\mathbf{x}_0)=p(\mathbf{x}_0,s;\mathbf{x})$ to $O(\varepsilon^2)$, as required.

[1] J. E. Gretz, A. O. Anderson, and S. Shaw, Immunol. Rev. **156**, 11 (1997).
[2] A. A. Itano and M. K. Jenkins, Nat. Immun. **4**, 733 (2003).
[3] M. Sixt, N. Kanazawa, M. Selg, T. Samson, G. Roos, D. P. Reinhart, R. Pabst, M. B. Lutz, and L. Sorokin, Immunity **22**, 19 (2005).
[4] J. N. Blattman, R. Antia, D. J. D. Sourdive, X. Wang, S. M. Kaech, K. Murali-Krishna, J. D. Altman, and R. Ahmed, J. Exp. Med. **195**, 657 (2002).
[5] P. Bousso and E. Robey, Nat. Immun. **4**, 579 (2003).
[6] M. J. Miller, S. H. Wei, I. Parker, and M. D. Cahalan, Science **296**, 1869 (2002).
[7] M. J. Miller, S. H. Wei, M. D. Cahalan, and I. Parker, Proc. Natl. Acad. Sci. U.S.A. **100**, 2604 (2003).
[8] M. J. Miller, A. S. Hejazi, S. H. Wei, M. D. Cahalan, and I. Parker, Proc. Natl. Acad. Sci. U.S.A. **101**, 998 (2004).
[9] T. R. Mempel, S. E. Henricksen, and U. H. von Andrian, Nature (London) **427**, 154 (2004).
[10] F. Castellino, A. Y. Huang, G. Altan-Bonnet, S. Stoll, C. Scheinecker, and R. Germain, Nature (London) **440**, 890 (2006).
[11] S. H. Wei, I. Parker, M. J. Miller, and D. Cahalan, Immunol. Rev. **195**, 136 (2003).
[12] J. Delon, S. Stoll, and R. N. Germain, Immunol. Rev. **189**, 51 (2002).
[13] C. C. Norbury, D. Malide, J. S. Gibbs, J. R. Bennink, and J. W. Yewdell, Nat. Immun. **3**, 265 (2002).
[14] E. Ingulli, A. Mondino, A. Khoruts, and M. K. Jenkins, J. Exp. Med. **185**, 2133 (1997).
[15] D. M. Catron, A. A. Itano, K. A. Pape, D. L. Mueller, and M. K. Jenkins, Immunity **21**, 341 (2004).
[16] G. I. Bell, J. Theor. Biol. **29**, 191 (1970).
[17] P. Wood, *Understanding Immunology* (Pearson Education Limited, Harlow, Essex, UK, 2001).
[18] S. A. Rice, *Comprehensive Chemical Kinetics Volume 25: Diffusion-Limited Reactions* (Elsevier, Amsterdam, 1985).
[19] M. Smoluchowski, Z. Phys. Chem., Stoechiom. Verwandtschaftsl. **92**, 129 (1917).
[20] M. Tachiya, Radiat. Phys. Chem. **21**, 167 (1983).
[21] H. G. Othmer, S. R. Dunbar, and W. Alt, J. Math. Biol. **26**, 263 (1988).
[22] G. H. Weiss, *Aspects and Applications of Random Walks* (North-Holland, Amsterdam, 1994).
[23] A. M. Berezhkovskii, Y. A. Makhnovskii, and R. A. Suris, J.

Stat. Phys. **65**, 1025 (1991).
[24] P. M. Richards, Phys. Rev. Lett. **56**, 1838 (1986).
[25] R. Bearon and T. Pedley, Bull. Math. Biol. **62**, 775 (2000).
[26] C. S. Patlak, Bull. Math. Biophys. **15**, 311 (1953).
[27] T. Hillen and H. G. Othmer, SIAM J. Appl. Math. **61**, 751 (2000).
[28] M. R. Spiegel, *Theory and Problems of Vector Analysis* (McGraw-Hill, New York, 1974).